



Weld penetration control of wire-filled pulsed gas tungsten arc welding of pipe in the horizontal position

Zhijiang Wang^{1,2} · Zitong Zeng^{1,2} · Shaojie Wu^{1,2} · Xinxin Shu³ · Chengfeng Wu^{1,2} · Dongpo Wang^{1,2} · Shengsun Hu^{1,2}

Received: 6 August 2022 / Accepted: 12 March 2023 / Published online: 23 March 2023
© International Institute of Welding 2023

Abstract

Wire-filled pulsed gas tungsten arc welding (GTAW-P) is usually used to join pipes in the horizontal position, in which uniform full penetration is required to guarantee a high weld quality. Based on the characteristic signals reflecting the penetration degree, the penetration control strategy of step welding is designed, and the dynamic modeling of backside molten pool width using the characteristic signals is conducted by back propagation (BP) neural network. The influence of step distance on the characteristic signals is explored. The weld is well shaped when the step distance is 3 mm. The backside weld width in the horizontal position can be controlled to be around the preset value with the control strategy of step welding and real-time feedback from the prediction of BP neural network. The control system is robust, which can work well under the fit-up condition of variable gap or variable heat dissipation in the horizontal welding of pipe.

Keywords Backside weld width · BP neural network · Step welding · Horizontal position · Wire-filled pulsed gas tungsten arc welding

1 Introduction

Pulsed gas tungsten arc welding (GTAW-P) has advantages of high quality and low cost, which is widely used in the pipe welding. In the pipe welding production, it is usually necessary to use wire-filled GTAW-P in the horizontal (2G) position, and uniform full penetration is required to obtain a high weld quality. Recently, the relationship between dynamic behavior of molten pool and penetration degree of stationary wire-filled GTAW-P of pipe in the horizontal position was studied in our previous study [1], in which the characteristic signals reflecting the occurrence of critical penetration and penetration degree were found. As per the

proposed characteristic signals in our previous study [1], the weld penetration of pipe in the horizontal welding may be controlled.

Weld penetration control is a challenging topic in welding field, which can be traced to 1970s [2]. To well implement the feedback control of weld penetration, reliable and easy-obtained feedback signals from the topside of weld pool are crucial as the weld penetration is indeed not visible from topside, and the backside of weld pool is usually not easily accessed. Thus, many sensing methods have been studied to get the characteristic signals from the arc/topside of weld pool to represent the weld penetration states, such as infrared technique [3–6], radiography [7], ultrasonography [8], and acoustic emission [9]. However, the foregoing sensing methods have their disadvantages, such as expensive equipment [7, 8], heterogeneous background noise [9], and radiation [7]. In contrast, visual method [10], which can obtain much intuitive information from the weld pool, and through-the-arc [11], which takes advantages of the heat source, i.e., arc itself instead of additional auxiliary sensing system, draw more and more attentions.

Visual sensing can directly obtain the geometric shape information of weld pool. There are many studies on the control of weld shaping by using visual sensing. In Refs. [12,

Recommended for publication by Commission XII - Arc Welding Processes and Production Systems

✉ Zhijiang Wang
wangzj@tju.edu.cn

¹ Tianjin Key Laboratory of Advanced Joining Technology, Tianjin 300354, China

² School of Materials Science and Engineering, Tianjin University, Tianjin 300354, China

³ Offshore Oil Engineering Co., Ltd, Tianjin 300452, China

[13], a 2-input (topside weld depression and width) 2-output (welding current and arc length) model of gas tungsten arc welding (GTAW) was established, and the weld penetration was controlled by a generalized predictive control algorithm. Liu and Zhang [14] established the relationship between geometric parameters of molten pool and welding parameters through dynamic tests and proposed a predictive control algorithm based on the linear system model to control the width, length, and convexity of GTAW molten pool. Zhang and Zhang [15, 16] studied the adjustments of the welding current after the welder observed the width, length, and convexity of molten pool and established a linear regression model based on the data of molten pool morphology and welder's adjustments. However, the decision-making and the adjustments of welder are nonlinear and fuzzy; the linear regression model is not good enough to track them. Liu et al. [17, 18] used the adaptive neuro-fuzzy inference system (ANFIS) to model the change in three-dimensional molten pool shape and welder's adjustments of welding current. The experimental results showed that ANFIS has a higher prediction accuracy than the linear regression model. Fan et al. [19] designed a three-optical-path vision system, which can simultaneously obtain the images of topside and backside molten pool in the wire-filled GTAW-P of aluminum alloy, and used an edge extraction algorithm to obtain the geometric information of molten pool. The designed proportional integral derivative (PID) controller can control the uniformity of weld penetration [19]. Chen et al. [20] established a linear model predictive controller (MPC) to control the stationary GTAW-P and obtained a weld with uniform backside weld width by step welding [20]. However, visual sensing will make the control system complex, and the image quality in visual sensing is easy to be affected in the welding processes.

The molten pool always oscillates in the welding process, which is closely related to the volume of molten pool and weld penetration states [21–24], and the oscillation of molten pool will directly affect the arc length/voltage. Therefore, the information of molten pool oscillation and weld penetration degree may be extracted from the arc voltage signal. Wang et al. [25] studied the relationship between the oscillation frequency of molten pool and the backside molten pool width in the stationary GTAW welding, and successfully realized the real-time control of backside weld width by step welding. Yang and He [26] superimposed a constant-frequency sine wave on the DC current to make the molten pool oscillate. When the natural oscillation frequency of molten pool is consistent with the frequency of sine wave, the molten pool resonates that can be reflected in the arc voltage signal, which is used for continuous weld penetration control in the autogenous GTAW welding [26]. Wang et al. [27] photographed the weld pool surface of pulsed gas metal arc welding (GMAW-P) with a high-speed

camera and collected the arc voltage signal at the same time. It was found that the change in weld pool surface height during the peak current period was related to the penetration degree, and the weld pool surface height directly affected the arc length/voltage, so the fluctuation of arc voltage during the peak current period (ΔU) can be used to predict penetration degree and can be well characterized by a linear model [27]. Based on this, Wang et al. [28] used an adaptive interval model control algorithm to control the weld penetration in GMAW-P. The controller took ΔU as the input and the base current duration (t_b) as the output to control the weld penetration in GMAW-P, in which process the controlled weld penetration was uniform [28]. Zou et al. [29] found that using the quotient of ΔU and the average voltage (\bar{U}) during the peak current period as the characteristic signal to characterize the penetration degree has a higher accuracy. An adaptive predictive control algorithm based on Hammerstein model was designed to control the penetration degree [29]. It provides an idea for multi-information fusion sensing. Cao et al. [30] fused the ΔU and \bar{U} , performed Kalman filtering to obtain the characteristic signal ΔU_{kf} representing the penetration degree, and used the second-order nonlinear autoregressive moving average model with exogenous inputs (NARMAX) to describe the relationship between ΔU_{kf} and base current (I_b). The controller had a good performance [30]. Similar to gas metal arc welding, some researchers studied the arc voltage sensing in GTAW. Li et al. [31] found that in GTAW-P, the surface of molten pool first expands to the direction of tungsten (i.e., the height of molten pool surface increases) and will be far away from the tungsten when critical penetration occurs. Therefore, the change in arc length caused by the change in the molten pool surface will lead to the change in arc voltage. Based on this, Li and Zhang [32] designed a predictive control algorithm, which can effectively drive the arc voltage to track the set value. At the same time, the welder's operation error can be compensated by adjusting the welding current in real time to avoid welding defects. The control system could obtain a weld with uniform weld penetration [32]. Cheng et al. [33] analyzed the stationary GTAW-P process and found the similar molten pool behaviors as those in Ref. [31]. When full penetration occurs, the arc voltage first decreases and then increases. By detecting the minimum arc voltage, the weld penetration was well controlled as per step welding [33]. Zhang et al. [34] studied the stationary GTAW-P and found that when critical penetration occurs, the oscillation amplitude of the molten pool surface during the peak current period will increase, resulting that the fluctuation of arc voltage during the peak current period rises significantly, and this characteristic signal can be used for weld penetration control. In summary, the arc voltage and its change, involved in time and frequency domain, were used to characterize and to control the weld penetration in the pulsed GTAW/GMAW

welding, which has showed its advantage over the vision sensing, because they are easier to obtain and to process at the manufacturing sites. Therefore, it is a promising way to control the weld penetration.

However, most researches focused on the flat (1G) welding position. A few of researches focused on other positions; for example, Rider [35] estimated the weld penetration depth for different positions by sensing the heat input to obtain the weld pool volume and sensing the topside weld width using a linear array of silicon photodiodes as the sensor, and controlled it in real time; in Refs. [31, 32], the weld penetration for all-position (5G) welding of pipe was controlled by using the arc voltage; in Ref. [36], a pipe inner inspection robot equipped with CMOS sensor and laser scanner was developed to monitor and to control the weld penetration of the nuclear steel pipe (5G position). In the horizontal welding position, the gravity is counteracted by the support and friction of the groove (or the workpiece), etc. Its weld pool oscillation will be affected by the arc; thus, our previous study [1] did a research on the molten pool behaviors in the horizontal welding and found that the characteristic signal ΔU^* (i.e., the change in average peak voltage) can reflect the occurrence of critical penetration, and the characteristic signals \overline{U}_b (i.e., the average base voltage) and ΔU_b (i.e., the fluctuation of base voltage) can reflect the backside molten pool width of stationary wire-filled GTAW-P of pipe in the horizontal position.

In the present work, a penetration control strategy based on the characteristic signals from our previous study [1], which can avoid the complexity of visual sensing, is proposed in Section 2. As per step welding that is usually employed in the condition with the characteristic signal sensed from the stationary welding, a weld penetration control system is established. Back propagation (BP) neural network is used to model the relationship between characteristic electrical signals and backside molten pool width (Section 3), so as to realize the real-time feedback control of full penetration of pipe in the horizontal position (Section 4). The conclusions are given in Section 5.

2 Experimental design and control strategy

Characteristic signals ΔU^* , \overline{U}_b , and ΔU_b proposed in previous study [1] were collected from the stationary welding, which may fail when continuous welding is conducted. For example, ΔU^* and ΔU_b will be affected by the change in weld pool shape and constriction of the pool by the workpiece, etc. which are seriously influenced by the welding process parameters/conditions and its resultant temperature distribution. Therefore, stationary welding condition was kept in the present work, and the step welding method, which usually handles such case, is employed to be used to

control the weld penetration of pipe in real time. However, in the typical stationary welding of the step welding process, the partial substitution of workpiece by the previous welding point with a high temperature may fail the characteristic signals, which needs to be well investigated. Figure 1 is the schematic diagram of the weld penetration control system. After the wire feeding of the stationary welding is finished, the critical penetration is first judged according to ΔU^* . As there is an abrupt change in average peak voltage when critical penetration occurs, ΔU^* is over the threshold (approximately 1 V) only in the critical penetration moment, i.e., detecting the moment with “ $\Delta U^* > \text{threshold}$ ” can be used for the judgement of critical penetration. And then the backside molten pool width \widehat{D}_3 is calculated in real time according to \overline{U}_b and ΔU_b by using the BP neural network, whose structure, parameters, and the corresponding effect are investigated later. When \widehat{D}_3 reaches the set backside molten pool width D_3^* , the controller will output a step signal by the data acquisition card to control the rotation of pipe and wire feeding to start a new stationary welding process at next welding point. The weld pool grows gradually as the heat input accumulates; therefore, when the arc is moved away from the present welding point by the step signal, the weld pool will solidify with the dimension \widehat{D}_3 or a little bit larger than that due to the thermal lag. The thermal lag should be assessed. If a large dimensional error is induced by the thermal lag, a predictive controller may be required, else the controller only needs to output the step signal in time. A continuous full-penetrated weld can be obtained by controlling the full penetration for each point and by overlapping the resulted full-penetrated welding points.

The step welding experiment system for the weld penetration control of wire-filled GTAW-P of pipe in the horizontal position is shown in Fig. 2. The welding torch was kept stationary, and the pipe was placed vertically on the three-jaw chuck (Model: K11/100), which was connected with the stepper motor (Model: 86) to realize the rotation of pipe. The stepper motor was controlled by the pulse signals from programmable logic controller (PLC, Model: S7-200) to achieve the movement from one welding point to the next one. The switches of PLC and wire feeder were connected to the normally open (NO) ports and COM ports of the two relays (Model: JQC-3FF-S-Z), respectively. The wire feeding time (for one welding point in the step welding) was 1 s when the arc started,

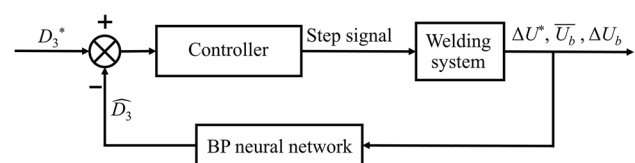


Fig. 1 Schematic diagram of the weld penetration control system

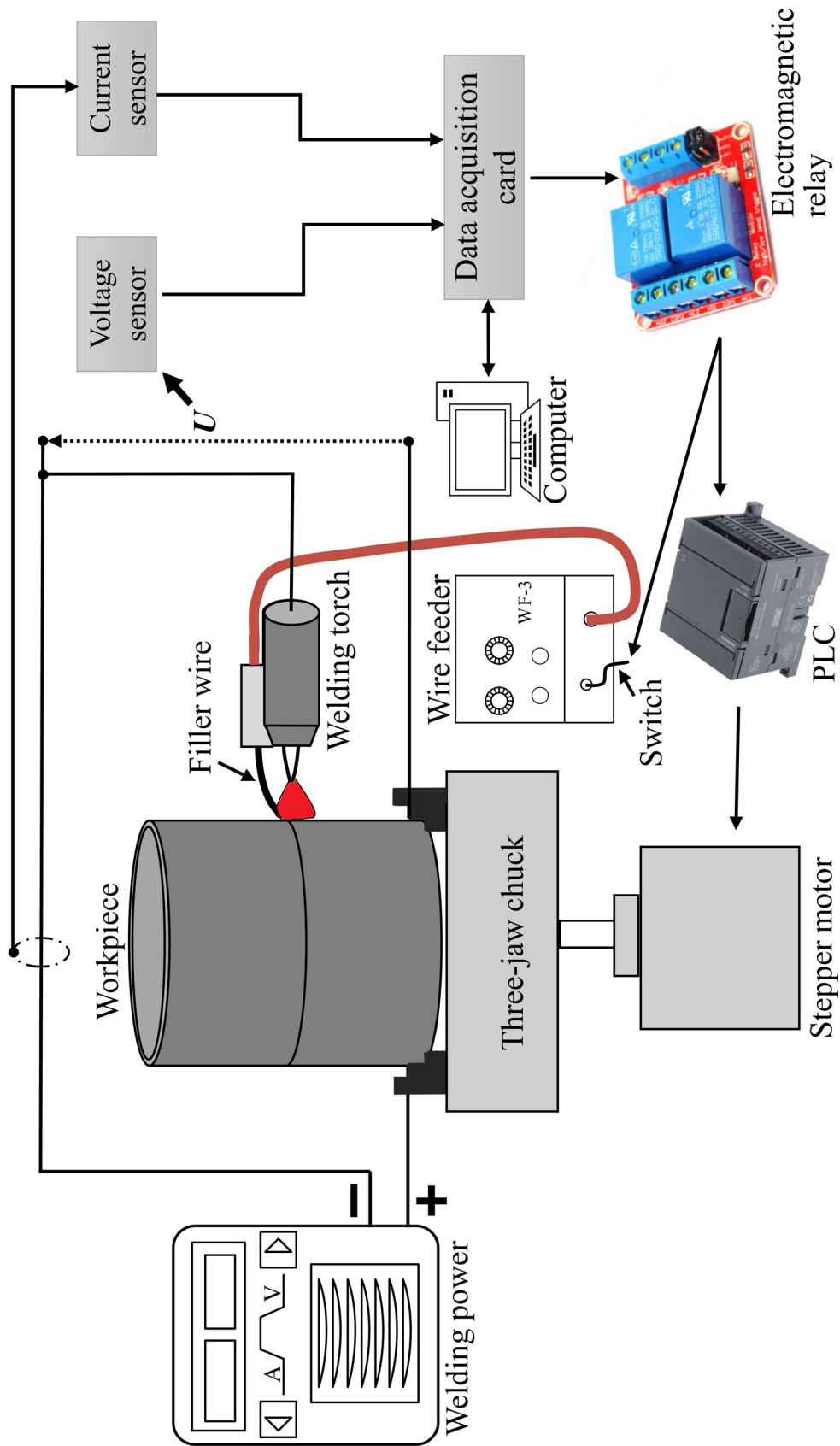


Fig. 2 Experimental system

which was controlled by a timer. The relays were triggered by the analog voltage signals outputted by the data acquisition card (Model: NI PCI-6221). Simulink Desktop Real-Time toolbox in MATLAB was employed to design the controller, which can drive the data acquisition card to acquire and output analog signals and digital signals. Hall sensors CHB-500SG and CHV-25P/50 were used to measure welding current and arc voltage signals, respectively.

The Fronius MagicWave 4000 welding machine was used as the power supply, and the peak current, base current, pulse frequency, and duty cycle were fixed at 150 A, 12 A, 5 Hz, and 50%, respectively. The workpiece and tungsten electrode were connected to the positive and negative poles of the power supply, respectively. The wire feeder was WF-3 produced by CK Worldwide Company, and the wire feed speed was 80 cm/min. The base metal were pipes of Q235B mild steel with a diameter of 100 mm and with a wall thickness of 2 mm. The welding wire was MG50-6 with a diameter of 1.2 mm. The chemical composition of base metal and filler wire is shown in Table 1. The diameter of tungsten electrode was 2.4 mm. The tungsten electrode was perpendicularly placed to the pipe, and the distance between the tungsten electrode and workpiece was kept at 4 mm. The filler wire was fed from the side and had an angle of approximately 90° with the electrode. The distance between filler wire and workpiece was 0.5 mm to ensure that the droplets are transferred in the stable bridging transfer mode. Argon with a purity of 99.99% was selected as the shielding gas, and its flow rate was 10 L/min.

To better describe the weld shaping with regard to the circumferential position, the start point of the stepping welding is defined the position of 0 o'clock, while the opposite side of the pipe is defined as the position of 6 o'clock. The torch will return to the position of 0 o'clock when the stepping welding ends.

3 Prediction model of backside weld width

The backside weld pool width has a relationship with \overline{U}_b and ΔU_b between the weld pool states of critical penetration and over penetration, as reported in our previous study [1]. They presented as approximately linear relationships, but the relationships were statistical. During the modeling work, the signal was filtered before it was used. Therefore, they are not strict linear relationships for static model, let alone the dynamic one. As well known, the actual welding process is nonlinear, time-varying, coupled with multiple factors, and with time delay,

etc.; thus, neural network is preferred to model the backside weld width in real time.

BP neural network has a strong nonlinear mapping and generalization ability and is widely used in engineering. In this paper, a BP neural network will be used to establish the model of backside molten pool width using the characteristic signals.

3.1 Samples selection

In order to improve the model accuracy of the BP neural network, it must be trained with sufficient training data. \overline{U}_b , ΔU_b , and the corresponding backside molten pool width D_3 were collected synchronously, as described in Ref. [1], by using the Hall voltage sensor and high-speed camera (Model: Photron FASTCAM Super 10KC) during the stationary welding process, which were then used as sampling data. Fifteen groups of stationary welding tests were conducted under the conditions in Section 2, and in each group, 20 sets of data from different sampling points were extracted. Then, 300 sets of sampling data were obtained, among which 250 sets of data were randomly selected as training samples, and the remaining 50 sets of data were used as validation samples.

Preliminary statistical analyses on the relationship between the input (\overline{U}_b and ΔU_b) and output (D_3) were discussed in our previous study [1], which indicated that \overline{U}_b increased almost linearly with the increase in D_3 , while ΔU_b also showed an increasing trend. Due to the thermal inertia in the welding process, the backside molten pool width corresponding to the characteristic signals has a hysteresis. The input layer of the neural network includes the average base voltage during the present current period ($\overline{U}_b(t)$), the average base voltage during the previous current period ($\overline{U}_b(t-1)$), the fluctuation of base voltage during the present current period ($\Delta U_b(t)$), and the fluctuation of base voltage during the previous current period ($\Delta U_b(t-1)$). The output layer of the neural network is the backside molten pool width (\widehat{D}_3). The neural network model is constructed according to the above-mentioned inputs and output, as shown in Fig. 3.

3.2 Parameter determination for BP neural network

The neural network model used in this paper has three layers. The number of nodes in the hidden layer, activation function, and training parameters need to be further determined.

Table 1 Chemical composition of the base material and filler wire (wt.%)

Elements	C	Mn	P	S	Si	Cu	Fe
Q235B	0.18	0.50	≤0.045	≤0.045	≤0.30	-	Balance
MG50-6	0.07	1.27	0.015	0.014	0.76	0.15	Balance

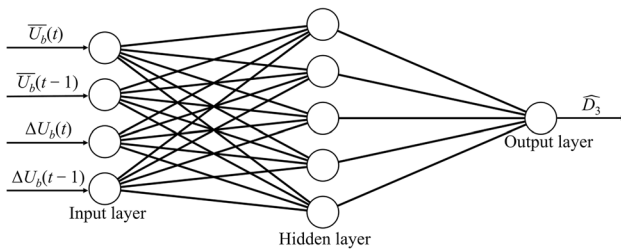


Fig. 3 Structure of BP neural network model

3.2.1 Number of nodes in the hidden layer

Setting an appropriate number of nodes in the hidden layer is important for the performance of BP neural network. For obtaining the optimal number of nodes in the hidden layer, the following formulae [37] can be referred to:

$$n_1 < \sqrt{n + m} + a \quad (1)$$

$$n_1 = \log_2 n \quad (2)$$

where n_1 is the number of nodes in the hidden layer, n is the number of nodes in the input layer, m is the number of nodes in the output layer, and a is a constant between 1 and 10. The maximum value $n_{1max} = 9$ and the minimum value $n_{1min} = 2$ for the number of nodes in the hidden layer were determined by the Eqs. (1) and (2). The neural networks with 2 to 9 nodes in the hidden layer were trained one by one. The root mean squared error (RMSE) of the validation samples were used to analyze the model error. The formula of RMSE is as follows:

$$RMSE = \sqrt{\frac{\sum_{i=1}^N (X_{obs,i} - X_{model,i})^2}{N}} \quad (3)$$

The RMSEs for the neural networks with 2 to 9 nodes in the hidden layer were compared, and the optimal number of nodes in the hidden layer for the final structure of BP neural network were determined as that for the neural network model with the minimum RMSE.

3.2.2 Activation function

The activation function can limit the output of neuron nodes to some range and introduce nonlinear ability. The inputs and outputs of purelin activation function can be arbitrary values, which is suitable for data fitting. Therefore, the purelin function was selected as the activation function, and the gradient descent method was used to train the neural network.

3.2.3 Training parameters

The training times, the learning rate, and the minimum error of the training target were set as 10,000, 0.001, and 0.00001 mm, respectively. When the number of training iterations reaches 10,000 or the training error is less than 0.00001 mm, the training process ends.

Based on the above-mentioned settings, the neural networks with 2 to 9 nodes in the hidden layer were trained, whose RMSEs are shown in Table 2. When the number of nodes in the hidden layer was set to 5, the RMSE was the smallest, which was 0.0799 mm. Therefore, the number of nodes in the hidden layer for the final structure of BP neural network was selected as 5.

3.3 Modeling results

Fifty samples were used to validate the BP neural network. The validation results are shown in Fig. 4. In Fig. 4a, the lower limit of D_3 in training dataset was 2 mm which is marked with the red dot dash line; while the upper limit was 10 mm, which was marked with the red dash line. In practice, if D_3 is lower than 2 mm, the weld is partially penetrated, while if D_3 is over 10 mm, the weld is over penetrated; thus, the training dataset covered the whole working range for full penetration condition. In other words, the BP neural network trained using the training dataset had the same working range, i.e., D_3 was within [2, 10] mm. All the validation samples were all in this range too, as shown in Fig. 4a. The maximum error was no more than 0.10 mm (Fig. 4b). It proved a high prediction accuracy of the model, showing a good model performance within the working range. Therefore, the BP neural network model can meet the requirements of predicting the penetration degree based on the characteristic signals.

4 Experimental results and discussion

4.1 The influence of step distance on characteristic signals

In our previous study [1], the relationship between characteristic signals and penetration degree in a single stationary welding was explored. In the step welding, the welding points overlap partially, and the previous welding point causes the change in temperature field of workpiece, which would influence the weld pool geometry

Table 2 RMSEs for the BP neural networks with 2 to 9 nodes in the hidden layer

Number of nodes in the hidden layer	2	3	4	5	6	7	8	9
RMSE/mm	0.1387	0.0910	0.0856	0.0799	0.0894	0.1023	0.1117	0.1317

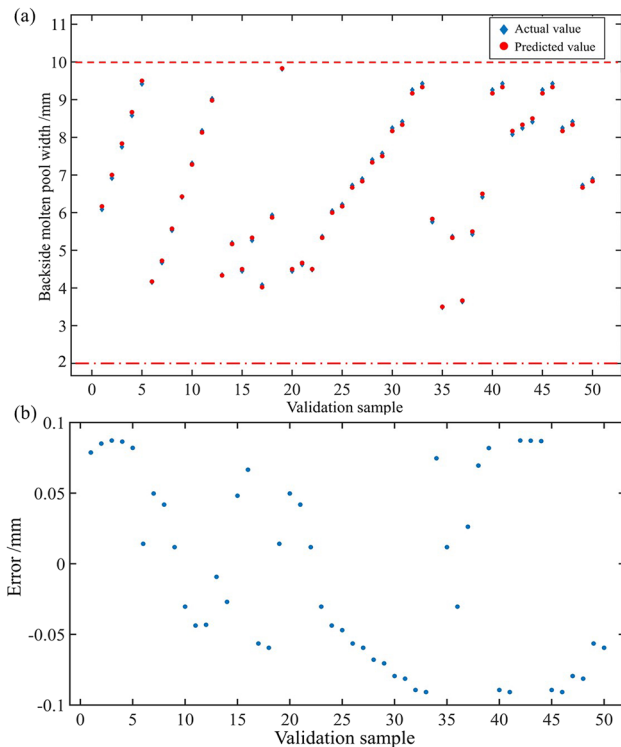


Fig. 4 Prediction results (a) and their errors (b) of BP neural network model

and its size of next point. Thus, the dynamic behavior of the present molten pool and the characteristic signals may also be interfered. In order to analyze the applicability of the characteristic signals obtained from the stationary welding in the step welding, four groups of welding tests with different step distances were conducted. The D_3^* was set to 5 mm, and the step distances were set as 7 mm, 5 mm, 3 mm, and 1 mm, respectively. When the step distance was 7 mm, the time for the torch travelling across this step distance was 35 ms (at an average torch travel speed of 200 mm/s relative to the workpiece), which was far less than the pulse current cycle of 200 ms. Therefore, the level of welding current during the torch travelling process was not considered.

The input and output of the feedback control system are shown in Fig. 5. Since the backside molten pool width was approximately 4 mm when critical penetration occurred [1], the start line of \widehat{D}_3 was set to 4 mm in Fig. 5. The step signals are in the form of pulse with an amplitude of approximately 4 V, which was sent to the stepper motor when the trigger condition is met. The weld morphology for the experiments in Fig. 5 is shown in Fig. 6.

When the step distance was 7 mm, there was almost no overlap between the neighbored welding points from the backside view (Fig. 6a2), while there was a small

part of welding points overlapped from the topside (Fig. 6a1). From Fig. 5a, \widehat{D}_3 obtained by the BP neural network gradually increased after the critical penetration occurred. When \widehat{D}_3 reached 5 mm, the control system sent a step signal to move the torch to the next position for a new stationary welding process, and in such a way, the backside weld width of each welding point was controlled to the preset value, approximately 5 mm. From the observations described above, the step distance of 7 mm between the welding points was too large, the previous welding point had no effect on the characteristic signals for the present one, but the backside weld width was uneven due to no overlap.

When the step distance was reduced to 5 mm, there was partial overlap between the adjacent welding points from the topside view (Fig. 6b1), and the uniform backside weld width (Fig. 6b2) was obtained, indicating that the previous welding point had little effect on the characteristic signals for the present one.

With the further decrease in the step distance to 3 mm, the overlap between the adjacent welding points increased from the topside view (Fig. 6c1), and the backside weld width was more uniform (Fig. 6c2) compared with the weld having a step distance of 5 mm. The influence of the previous welding point on the characteristic signals for the present one still can be neglected.

However, when the step distance was reduced to 1 mm, the volume of molten pool during the welding process increased (as can be inferred from Fig. 6d1 and 6d2, the topside and backside weld width increased) due to the heating of the previous welding point, and burn through occurs at approximately 30 s (Fig. 5d). From Fig. 5d, after approximately 15 s, there were some welding points with only one prediction from the BP neural network, indicating the significant influences of the previous welding point. It failed the prediction model using the proposed characteristic signals from the stationary welding, and further failed the control strategy of stepping welding.

To summarize, the step welding method is feasible, only if the step distance is set properly, in the horizontal position, in which condition the proposed characteristic signals and control strategy are effective. In the subsequent backside weld width control, the step distance controlled by the controller was all set to the optimized one, i.e., 3 mm.

4.2 Backside weld width control experiment

4.2.1 Step welding experiment with closed-loop control

The schematic diagram of the normally placed pipe is shown in Fig. 7. The square butt welding was conducted in the horizontal position. The set value in the step

Fig. 5 The input and output of the control system. The step distances were set as 7 mm (a), 5 mm (b), 3 mm (c), and 1 mm (d), respectively

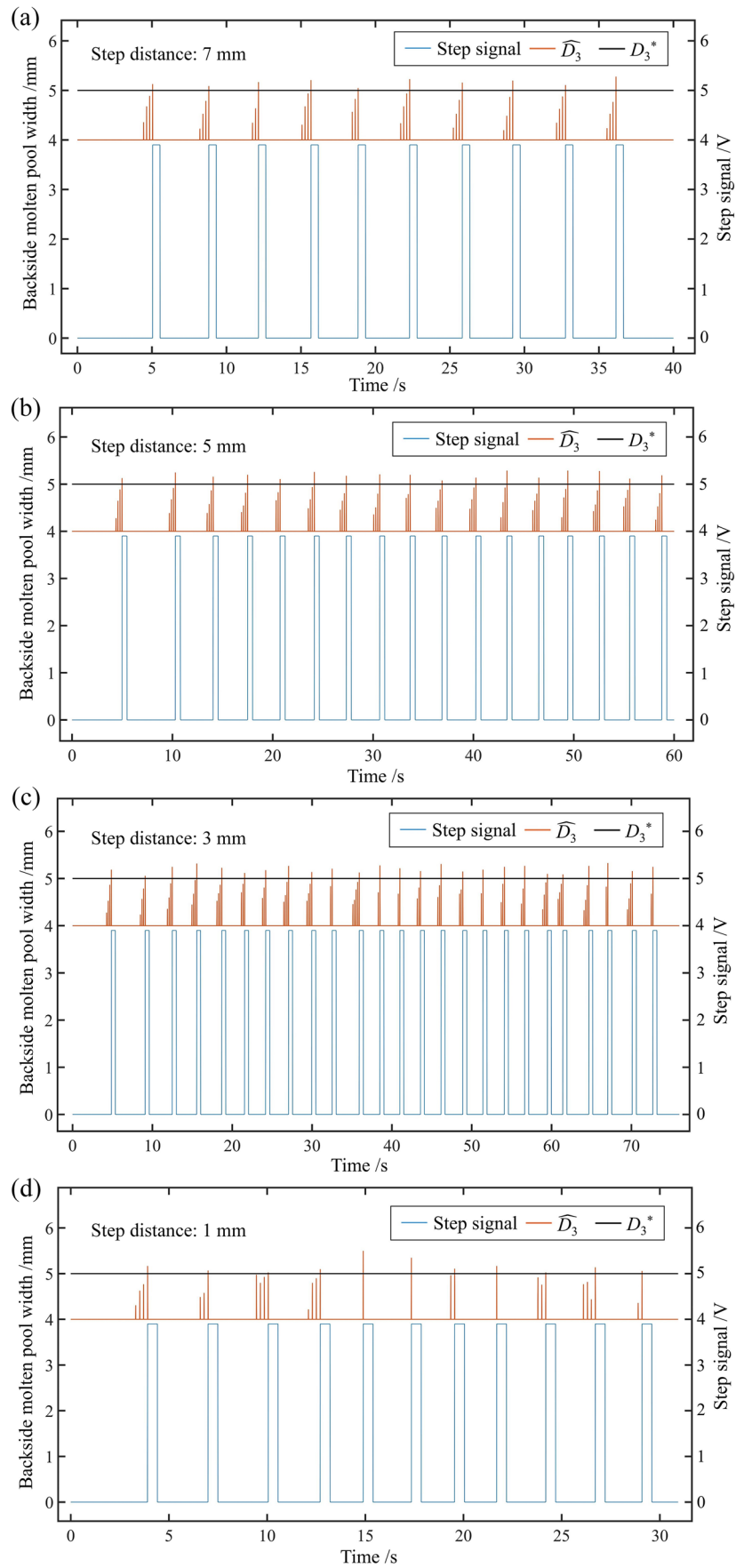


Fig. 6 The weld morphology. The topside weld appearances for experiments with the step distances of 7 mm (a1), 5 mm (b1), 3 mm (c1), and 1 mm (d1) are presented at left side; and the corresponding backside weld appearances are presented in subfigures a2–d2 at the right side, respectively

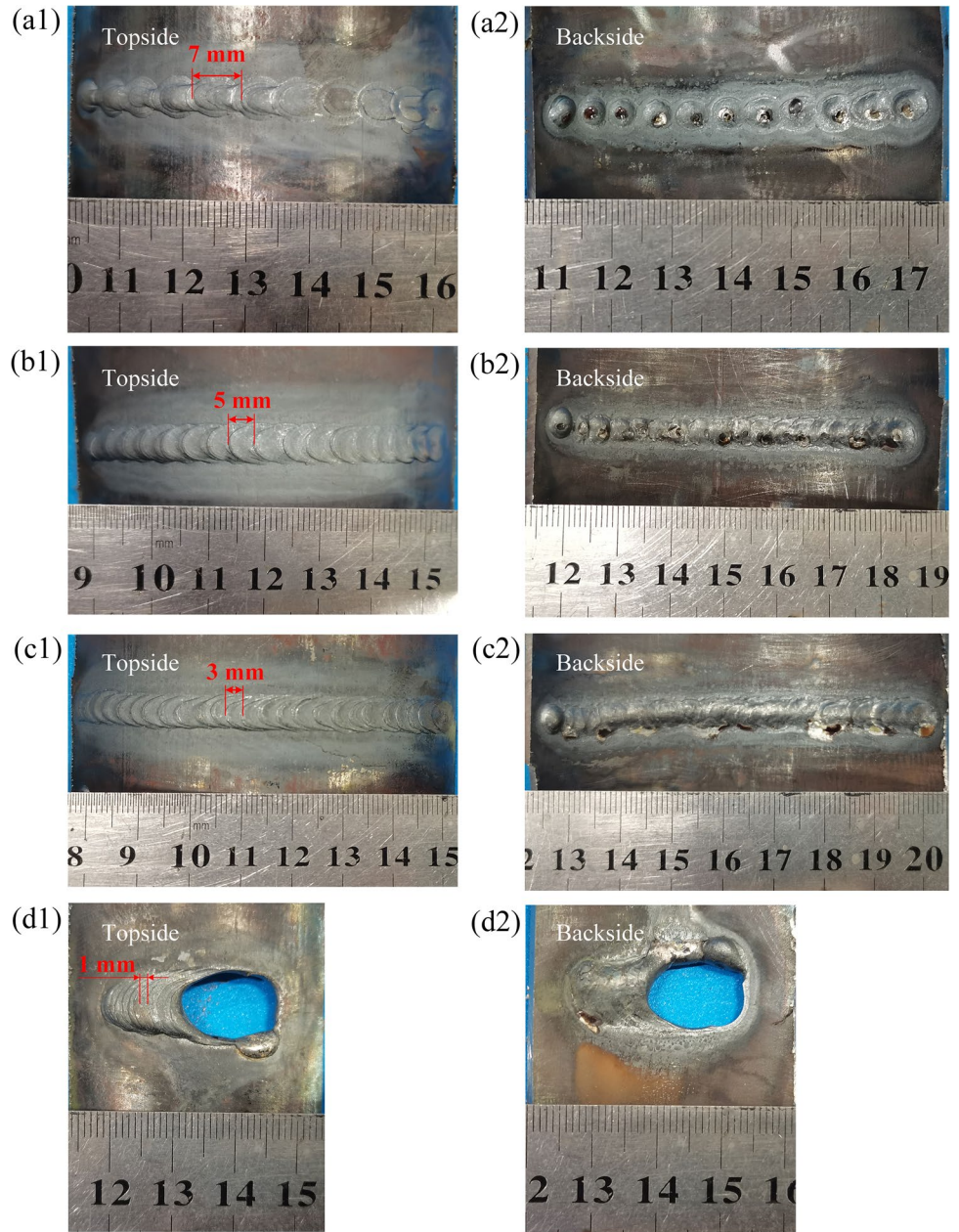


Fig. 7 Schematic diagram of normally placed pipe. **a** Main view; **b** vertical view

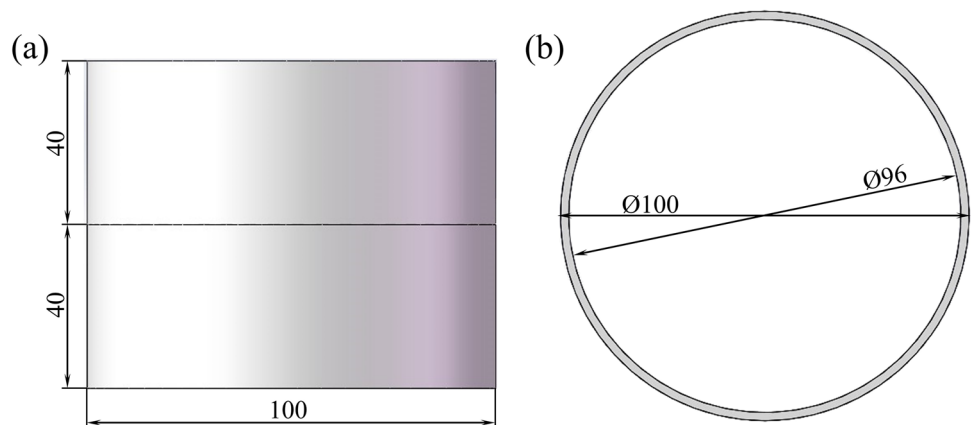
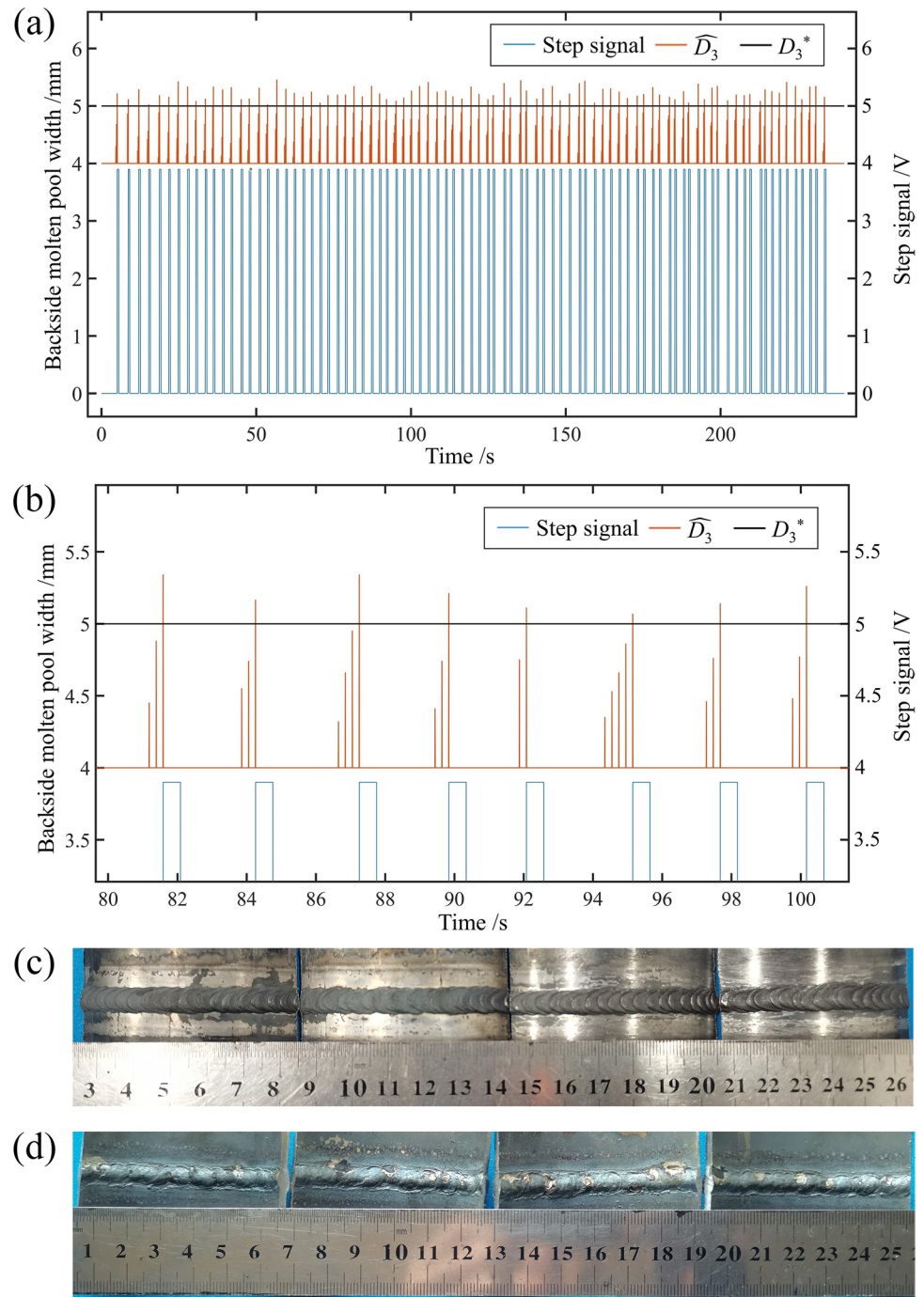


Fig. 8 The input and output of the control system and weld appearance in the step welding experiment with fixed backside weld width. **a** The input and output of control system; **b** enlarged view of **a** from 80 to 100 s; **c** topside weld appearance; and **d** backside weld appearance



welding experiment with closed-loop control was fixed, $D_3^* = 5$ mm, and the control results are shown in Fig. 8. Figure 8b is the enlarged view of the input and output of the control system from 80 to 100 s. When the backside molten pool width calculated by BP neural network reached 5 mm, the control system sent a step signal for the next stationary welding. In order to observe the weld shaping inside the pipe, the pipe was cut into 4 pieces. The topside and backside of the weld were well shaped,

and the backside weld width was uniform and maintained at approximately 5 mm. The experimental results showed that no predictive algorithm is needed for the controller.

In order to explore the regulation process of the control system, a test with variable set value of D_3^* was conducted. D_3^* stepped from 5 to 7 mm. The control results are shown in Fig. 9. After the D_3^* stepped to 7 mm, the control system sent a step signal when \widehat{D}_3 reached 7 mm, and the backside weld width was apparently stepped up at

the position with yellow arrow in Fig. 9d. The backside weld width was controlled to approximately 5 mm and approximately 7 mm before and after the step change, respectively. The experimental results showed that the regulation process cannot be clearly observed due to the intermittent control in the step welding, but the relationship between \overline{U}_b , ΔU_b , and the backside molten pool width works well when the step distance is set properly.

4.2.2 Robustness of the control system

To test the robustness of the control system, closed-loop control experiments with variable gap and variable heat dissipation were designed and conducted.

Figure 10 shows the schematic diagram of a pair of pipes under the fit-up condition of a variable gap. The minimum gap between the pipes was 0 mm (at 0 o'clock)

Fig. 9 The input and output of control system and weld appearance in the step welding experiment with variable backside weld width. **a** The input and output of control system; **b** enlarged view of **a** from 105 to 125 s; **c** topside weld appearance; and **d** backside weld appearance. The yellow arrow points to the step position in **d**

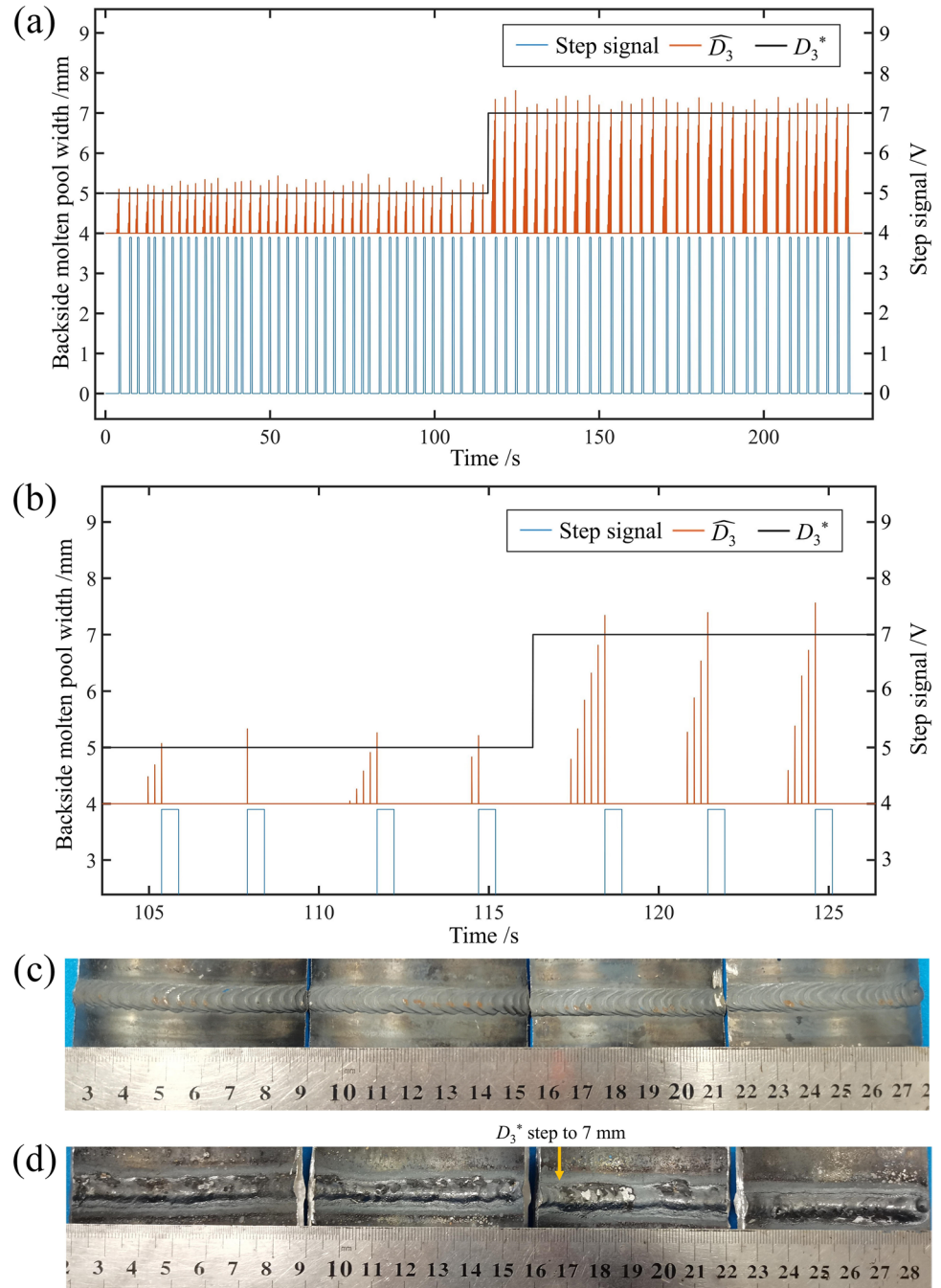


Fig. 10 Schematic diagram of pipes under the fit-up condition of a variable gap (in mm). **a** Main view; **b** left view

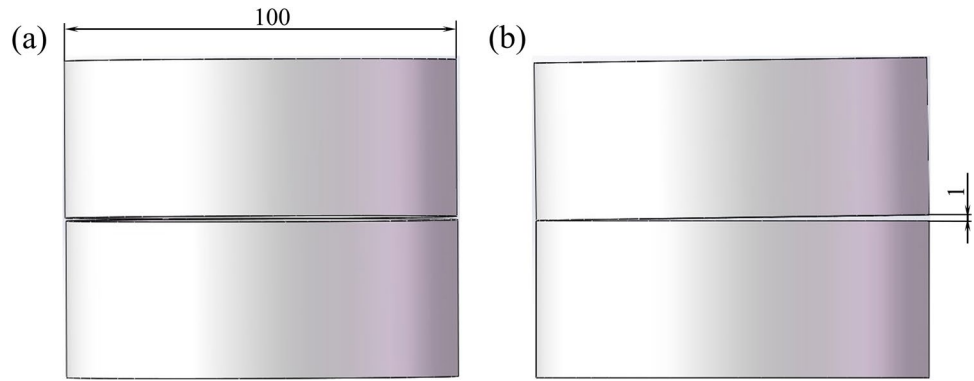


Fig. 11 The input and output of the control system and weld appearance in the step welding under the fit-up condition of a variable gap. **a** The input and output of the control system; **b** enlarged view of **a** from 80 to 100 s; **c** topside weld appearance; and **d** backside weld appearance

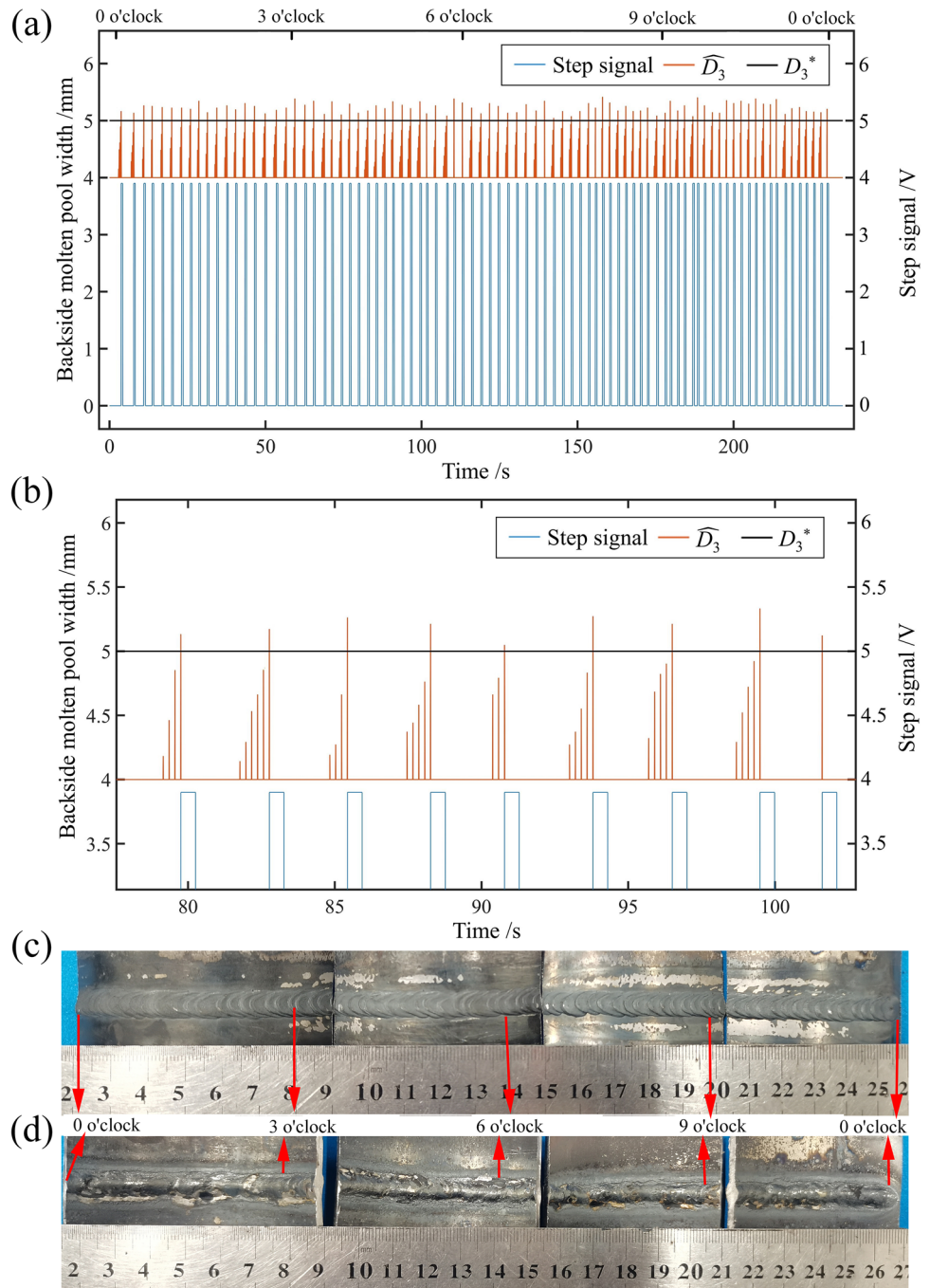
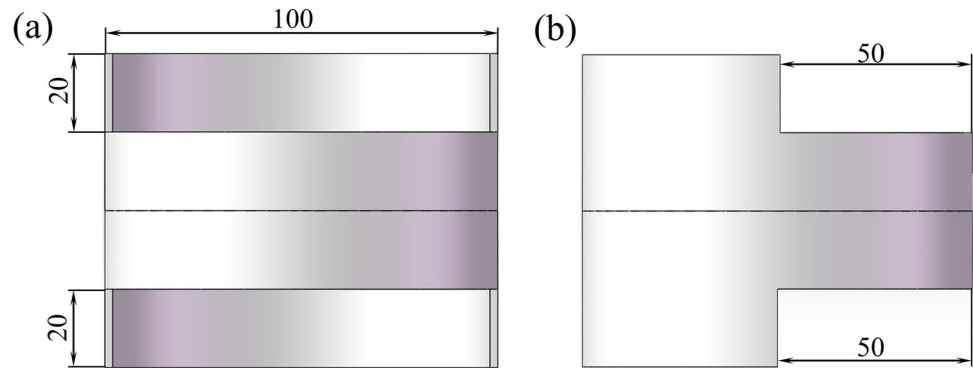


Fig. 12 Schematic diagram of pipes under the condition of variable heat dissipation (in mm). **a** Main view; **b** left view



and the maximum was 1 mm (at 6 o'clock). The set value was fixed, $D_3^* = 5$ mm, in the pipe joining process with variable gap under the condition shown in Fig. 10. The control results are shown in Fig. 11. The topside and backside of the weld were well shaped, and the backside weld width was uniform, approximately 5 mm. The control system mainly controls the backside molten pool width according to the molten pool states; thus, it can work well under the fit-up condition of a variable gap.

Variable heat dissipation condition was created by cutting slots on the upper and lower pipes (from position of 3 o'clock to 9 o'clock), as shown in Fig. 12. The set value was fixed, $D_3^* = 5$ mm. The control experiment was conducted in the pipe joining process with variable heat dissipation under the condition shown in Fig. 12. The control results are shown in Fig. 13. In areas with different heat dissipation conditions, the topside and backside of the weld were well shaped, and the backside weld width was maintained at approximately 5 mm. Therefore, the control system can work well under different heat dissipation conditions.

5 Conclusions and future work

This work mainly designed a penetration control system for the wire-filled pulsed gas tungsten arc welding (GTAW-P) of pipe in the horizontal position. BP neural network was used to model the relationship between the average base voltage (\bar{U}_b), the fluctuation of base voltage (ΔU_b), and the backside molten pool width (D_3). Step welding method was employed to verify the effectiveness of the control strategy. The main conclusions can be summarized as follows:

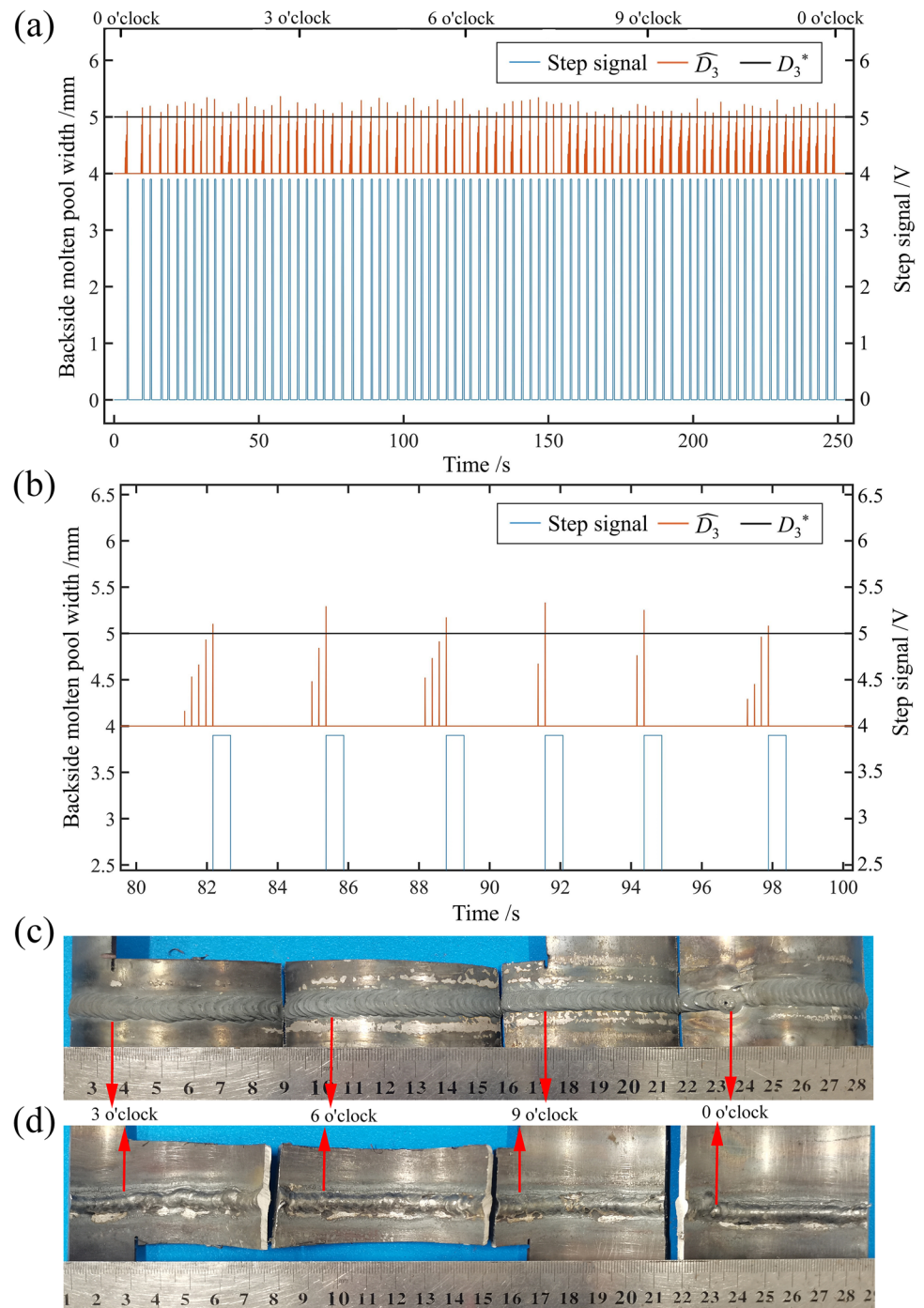
(1) As per step welding, a weld penetration control strategy was proposed and a weld penetration control

system was designed for the wire-filled GTAW-P of pipe in the horizontal position. The control strategy is that firstly, the occurrence of critical penetration is judged using the change in average peak voltage (ΔU^*) in the stationary welding, and then BP neural network is used to calculate the backside molten pool width (\widehat{D}_3) according to \bar{U}_b and ΔU_b , when \widehat{D}_3 reaches the preset value (D_3^*), the controller drives the stepper motor and wire feeder for a new stationary welding.

- (2) The BP neural network model with 5 nodes in the hidden layer and purelin function as the activation function was trained to model the relationship between \bar{U}_b , ΔU_b , and D_3 in real time, which had a high prediction accuracy with the maximum error no more than 0.10 mm.
- (3) It is verified that the characteristic signals was effective in step welding. When the step distance was 3 mm under the condition of the present work, the weld was well shaped and D_3 was uniform.
- (4) The closed-loop feedback control system with the BP neural network prediction model can effectively control D_3 to be around the set value. The control system mainly controls D_3 according to the molten pool states, due to which the control system can work with a strong robustness in the step welding, even under the condition of variable gap or variable heat dissipation.

In the present work, the mapping of input and output by BP neural network was obtained under the conditions that (a) the base material was Q235B; (b) the thickness of the base material was 2 mm; (c) the weld was penetrated and the backside weld width of it was in the range of 2 mm to 10 mm; etc. Thus, more modeling work should be done in the future so that the prediction model could be improved to handle more complex conditions.

Fig. 13 The input and output of the control system and weld appearance under the condition of variable heat dissipation. **a** The input and output of the control system; **b** enlarged view of **a** from 80 to 100 s; **c** topside weld appearance; and **d** backside weld appearance



Author contribution Zhijiang Wang: Conceptualization, methodology, formal analysis, resources, writing (review and editing), funding acquisition, project administration. Zitong Zeng: Methodology, software, formal analysis, investigation, data curation, visualization, writing—original draft. Shaojie Wu: Formal analysis, validation, writing—review and editing. Xinxin Shu: Formal analysis, validation. Chengfeng Wu: Methodology, software. Dongpo Wang: Supervision. Shengsun Hu: Writing—review and editing.

Funding This study is supported by the National Natural Science Foundation of China (Grant No.: 51505326) and Natural Science Foundation of Tianjin (Grant No.: 16JCQNJC04300).

Data availability The datasets generated during and/or analyzed during the current study are available from the corresponding author on reasonable request.

Code availability The codes are not publicly available due to the commercial restriction.

Declarations

Ethics approval Not applicable.

Consent to participate Not applicable.

Consent for publication The authors give their consent for the publication of identifiable details, which can include photograph(s) and/or videos and/or case history and/or details within the text to be published in *Welding in the World*.

Conflict of interest The authors declare no competing interests.

References

- Zeng ZT, Wang ZJ, Hu SS et al (2022) Dynamic molten pool behavior of pulsed gas tungsten arc welding with filler wire in horizontal position and its characterization based on arc voltage. *J Manuf Process* 75:1–12
- Boughton P, Rider G. 1978 Feedback control of weld penetration. *Welding Institute Conference Proceedings Advances in Welding Processes* 203–215
- Nagarajan S, Chen WH, Chin BA (1988) Welding penetration sensing and control. *Infrared Technology XIV* 972:268–272
- Chen W, Chin BA (1990) Monitoring joint penetration using infrared sensing techniques. *Weld J* 69(5):181s–185s
- Song JB, Hardt DE (1993) Closed-loop control of weld pool depth using a thermally based depth estimator. *Weld J* 72(10):471s–478s
- Farson DR, Richardson R, Li X (1998) Infrared measurement of base metal temperature in gas tungsten arc welding. *Weld J* 77(9):217s–226s
- Rokhlin SI, Guu AC (1990) Computerized radiographic sensing and control of an arc welding process. *Weld J* 69(3):83s–97s
- Carlson NM, Johnson JA (1988) Ultrasonic sensing of weld pool penetration. *Weld J* 67(11):239s–246s
- Liu X, Kannatry-Asibu E Jr (1990) Classification of AE signals for monitoring martensite formation from welding. *Weld J* 69(10):389s–394s
- Richardson RW, Gutow DA, Anderson RA et al (1984) Coaxial welding pool viewing for processing monitoring and control. *Weld J* 63(3):43s–50s
- Cook G E. 1983 Through-the-arc sensing for arc welding. *Proceedings of Tenth Conference on Production Research and Technology (NSF ISBN O-89883-087-7)* 141–151
- Zhang YM, Kovacevic R, Wu L (1996) Dynamic analysis and identification of gas tungsten arc welding process for weld penetration control. *Journal of Engineering for Industry* 118(1):123–136
- Zhang YM, Kovacevic R (1996) Adaptive control of full penetration gas tungsten arc welding. *IEEE Trans Control Syst Technol* 4(4):394–403
- Liu YK, Zhang YM (2013) Control of 3D weld pool surface. *Control Eng Pract* 21(11):1469–1480
- Zhang WJ, Zhang YM (2012) Modeling of human welder response to 3D weld pool surface: part I – principles. *Weld J* 91(11):310s–318s
- Zhang WJ, Zhang YM (2012) Modeling of human welder response to 3D weld pool surface: part II – results and analysis. *Weld J* 91(12):329s–337s
- Liu YK, Zhang YM, Kvidahl L (2014) Skilled human welder intelligence modeling and control: part I – modeling. *Weld J* 93(2):46s–52s
- Liu YK, Zhang YM, Kvidahl L (2014) Skilled human welder intelligence modeling and control: part II – analysis and control applications. *Weld J* 93(5):162s–170s
- Fan CJ, Lv FL, Chen SB (2009) Visual sensing and penetration control in aluminum alloy pulsed GTA welding. *Int J Adv Manuf Technol* 42(1–2):126–137
- Chen J, Chen J, Feng Z et al (2019) Model predictive control of GTAW weld pool penetration. *IEEE Robotics and Automation Letters* 4(3):2762–2768
- Madigan RB, Renwick RJ, Farson D et al (1986) Computer based control of full penetration GTA welds using pool oscillation sensing. *Computer technology in welding (TWI)* 165–174
- Deam RT (1989) Weld pool frequency a new way to define a weld procedure. *Recent trends in welding science and technology (ASM)* 967–971
- Xiao YH, den Ouden G (1990) A study of GTA weld pool oscillation. *Weld J* 69(8):289s–293s
- Anedenroomer AJR, den Ouden G (1998) Weld pool oscillation as a tool for penetration sensing during pulsed GTA welding. *Weld J* 77(5):181s–187s
- Wang QL, Yang CL, Geng Z (1993) Separately excited resonance phenomenon of the weld pool and its application. *Weld J* 72(9):455s–462s
- Yang CL, He JS (1999) Welding penetration control with weld pool resonance in traveling pulse TIG welding. *Transactions of the China Welding Institution* 20(4):251–257 (In Chinese)
- Wang ZJ, Zhang YM, Wu L (2010) Measurement and estimation of weld pool surface depth and weld penetration in pulsed gas metal arc welding. *Weld J* 89(6):117s–126s
- Wang ZJ, Zhang YM, Wu L (2012) Adaptive interval model control of weld pool surface in pulsed gas metal arc welding. *Automatica* 48(1):233–238
- Zou SY, Wang ZJ, Hu SS et al (2020) Control of weld penetration depth using relative fluctuation coefficient as feedback. *J Intell Manuf* 31:1203–1213
- Cao Y, Wang ZJ, Hu SS et al (2021) Modeling of weld penetration control system in GMAW-P using NARMAX methods. *J Manuf Process* 65:512–524
- Li XR, Shao Z, Zhang YM et al (2013) Monitoring and control of penetration in GTAW and pipe welding. *Weld J* 92(6):190s–196s
- Li XR, Zhang YM (2014) Predictive control for manual plasma arc pipe welding. *J Manuf Sci Eng* 136(4):041017
- Cheng YC, Xiao J, Chen SJ et al (2018) Intelligent penetration welding of thin-plate GTAW process based on arc voltage feedback. *Trans China Weld Inst* 39(12):1–4, 43 (In Chinese)
- Zhang SQ, Hu SS, Wang ZJ (2016) Weld penetration sensing in pulsed gas tungsten arc welding based on arc voltage. *J Mater Process Technol* 229:520–527
- Rider G (1986) Control of weld pool size and position. *Rob Weld* 217–226
- Wang LR, Wang SA, Liu WH et al (2021) In-process visual monitoring of penetration state in nuclear steel pipe welding. *Transactions on Intelligent Welding Manufacturing* 193–200
- Wang XC, Shi F, Yu L et al (2013) *MATLAB neural network - analyses of 43 cases (Chinese edition)*. Beijing University of Aeronautics and Astronautics Press

Publisher's note Springer Nature remains neutral with regard to jurisdictional claims in published maps and institutional affiliations.

Springer Nature or its licensor (e.g. a society or other partner) holds exclusive rights to this article under a publishing agreement with the author(s) or other rightsholder(s); author self-archiving of the accepted manuscript version of this article is solely governed by the terms of such publishing agreement and applicable law.